OPEN ACCESS

University of Dundee

University of Dundee

Diffraction and refraction of nonlinear waves by the Green-Naghdi equations

Hayatdavoodi, Masoud; Cengiz Ertekin, R.

Published in:
Journal of Offshore Mechanics and Arctic Engineering

Publication date:
2022

Document Version
Peer reviewed version

Link to publication in Discovery Research Portal

Citation for published version (APA):
Hayatdavoodi, M., & Cengiz Ertekin, R. (2022). Diffraction and refraction of nonlinear waves by the Green-Naghdi equations. *Journal of Offshore Mechanics and Arctic Engineering*.

General rights
Copyright and moral rights for the publications made accessible in Discovery Research Portal are retained by the authors and/or other copyright owners and it is a condition of accessing publications that users recognise and abide by the legal requirements associated with these rights.

• Users may download and print one copy of any publication from Discovery Research Portal for the purpose of private study or research.
• You may not further distribute the material or use it for any profit-making activity or commercial gain.
• You may freely distribute the URL identifying the publication in the public portal.

Take down policy
If you believe that this document breaches copyright please contact us providing details, and we will remove access to the work immediately and investigate your claim.

Download date: 11. Nov. 2022

Diffraction and refraction of nonlinear waves by the Green-Naghdi equations

Masoud Hayatdavoodi *
Civil Engineering Department
University of Dundee
Dundee, DD1 4HN, UK
& College of Shipbuilding Engineering
Harbin Engineering University
Harbin, China

R. Cengiz Ertekin †
Ocean and Resources Engineering Department
SOEST, University of Hawaii at Manoa
2540 Dole St., Holmes 402, Honolulu, HI 96822
& College of Shipbuilding Engineering
Harbin Engineering University
Harbin, China

Author Accepted Manuscript.
Not Copyedited by the Journal.

ABSTRACT

Diffraction and refraction of nonlinear shallow water waves due to uneven bathymetry are studied by use of the Green-Naghdi (GN) equations in three dimensions. A numerical wave tank consisting of deep, transitional and shallow regions is created. Various forms of three-dimensional bathymetry, consisting of ramps with nonuniform profiles and large slopes are used to connect the deep-water side of the tank to the shallow-water shelf. A wavemaker is placed at the upwave side of the domain, capable of generating solitary and cnoidal waves of the GN equations. A numerical wave absorber is located downwave of the domain to minimize the wave reflection back into the domain. The system of equations is solved numerically in time domain by use of a second-order finite difference approach for spatial discretization, and in a boundary-fitted coordinate system, and by use of the Modified Euler method for time marching.

*Address all correspondence to M. Hayatdavoodi (MHayatdavoodi@dundee.ac.uk).
†Fellow, ASME

Copyright © by ASME

Results include solitary and cnoidal wave surface elevation and particle velocities and are compared with the existing solutions where possible. Overall very good agreement is observed. Discussion is provided on the nonlinearity and dispersion effects on the wave diffraction and refraction by the various forms of the ramps, as well as on the performance of the GN equations in solving these problems.

Keywords: *Nonlinear shallow water waves, wave shoaling, refraction and diffraction, Green-Naghdi equations, solitary wave, cnoidal waves*

Introduction

Waves undergo significant deformation as they propagate from deep to coastal water and over variable seafloor. Wave diffraction and refraction are subjects of great interest to ocean engineers. Linear wave theory, based on the assumption of small amplitude waves, provides solutions to wave diffraction and refraction in the presence of simplified bathymetry and geometries. In shallow water, however, the water depth is much less than the wavelength, and the wave amplitude is not necessarily small when compared to the water depth, and hence the assumption of a linear free-surface boundary condition may no longer be applicable. Due to the change in water depth, the long waves undergo significant transformation. The original, nearly sinusoidal, wave profile transforms into waves of long and flat troughs and isolated and rather sharp crests as they enter shallow water. The wave height, speed and direction of propagation would also change significantly, and these vary with the spatial form of the bathymetry. Such deformations continue as the water depth decreases, to the limit that the wave becomes asymmetric about its crest and eventually leads to instabilities resulting in energy attenuation, formation of higher harmonics, and possibly wave breaking. The nonlinear effects resulting in such wave transformations cannot be captured by the simplified linear free-surface boundary conditions. Given the climate change and its impact on the frequency and intensity of extreme events, and the sea-level rise, it is becoming increasingly more important to develop approaches that can realistically and efficiently analyse wave transformation in coastal areas, and provide realistic information about the wave conditions as they approach shores and costal structures.

A common approach to model the nonlinear free-surface boundary condition is to assume that certain important features of the fluid domain remain unchanged during wave transformation, and thus to obtain an approximate solution for the nonlinear boundary conditions. In shallow water, this is achieved by introducing two major scales, namely nonlinearity (the ratio of wave height to water depth, $\sigma = H/h$) and dispersion (the ratio of water depth to wavelength, $\varepsilon = h/\lambda$). The unknowns (typically the velocity potential and the free surface) are expanded into a perturbation series ordered in terms of σ and ε, the scales or perturbation parameters, typically assumed small

Author's Accepted Manuscript, Not Copy-edited by the Journal.

 Copyright © by ASME

from the outset. It is then possible for one to decide whether σ or ε is more critical, and which terms in the expansion are to be retained and which terms can be discarded, determined based on the physical problem, and hence obtain an approximate solution to the exact problem. This is the "classical perturbation method" in water wave mechanics, and is followed by [1–8] and several others afterwards to obtain various forms of theories for nonlinear wave propagation in shallow water. All methods, following the perturbation approach, arrive at similar, but not identical, equations for the propagation of long waves. Models developed for wave diffraction and refraction in shallow water based on these approaches are discussed in [9–16], among others.

Green and Naghdi [17] proposed yet another fundamentally different approach in studying nonlinear wave transformation in shallow water based on a *continuum model* typically applied to the theory of plates and shells in structural mechanics. The theory is developed based on the directed or Cosserat surface, a deformable surface embedded in a Euclidean three-dimensional space to every point of which a deformable vector, called a director, is assigned. The Cosserat surface is three-dimensional in character, but only depends on two spatial dimensions and time. The directors of the Cosserat surface specify how certain properties are distributed in the third dimension of the *continuum model*. In this theory, the number of the directors defines the *Level* of the theory.

In the Level I theory, used in this study, the deformable medium is a body of sheet-like fluid consisting of a deformable top (free) surface and a single director attached to each point of the surface. This assumption, which is the only assumption made about the kinematics of the fluid sheet, is equivalent to the linear distribution of the vertical velocity along the water column, and hence (due to the continuity equation) the horizontal velocity becomes invariant over the water depth. This makes the Level I theory applicable to propagation of long waves. See, e.g., [18–22] for discussion on the range of applicability of various forms of the GN equations to nonlinear wave transformation.

Given that no perturbation is used in the derivation of the Green-Naghdi (GN hereafter) equations, there is no restriction on any scaling ratio, e.g., wave amplitude over the wave length, or alike in this approach, unlike the classical approximations. The only restriction on the thickness of the fluid sheet is that it is finite, and nonzero (zero water depth leads to a singularity in the equations). There is no need to define velocity potential and hence irrotationality of the flow is not necessary either. The GN equations are translationally (Galilean) invariant (unlike the equations presented by [3], among others), satisfy the nonlinear free surface boundary conditions and the conservation of mass exactly, and postulate the integrated momentum equation.

Further flexibility can be given to the directors when deriving the GN equations. This can be achieved by assuming higher-order functions (polynomial or exponential) for the distribution of the vertical velocity along

Author's Accepted Manuscript,
Not Copy-edited by the Journal.

 Copyright © by ASME

the water column. High-level GN equations are applicable to wave propagation in any water depth, see e.g. [21, 23–26]. We note that the boundary conditions are satisfied exactly by the GN equations of any level. That is, the only difference between the GN equations of different levels is on the velocity field.

The goal of this study is to investigate the effects of spatial and large changes of the bathymetry on the propagation of nonlinear waves in shallow water by use of the Level I GN equations. The GN model allows studying the wave transformation while preserving the effect of nonlinearity, dispersion and wave reflection (i.e., no need to restrict the wave motion to one direction only). To achieve this, various forms of bottom bathymetry with three dimensional (3D) effects on the wave field are considered in a systematic manner and discussion is provided on the wave transformation and effect of the bathymetry changes to the wave field. The 3D ramps are modified systematically, such that two of them are concave (where the middle of the ramp is deeper than the edges) and two are convex (where the edges of the ramp are deeper than the middle). Otherwise, the ramps dimensions and slopes, and the upwave and downwave water depths are invariant between these cases. Hence, any difference observed in transformation of the wave is due to the shape of the ramp (whether it is concave or convex), and how the form of the ramps affects the wave field. The theory and the solution are discussed first, followed by an introduction to the physical problems under consideration. Results of solitary and cnoidal wave diffraction and refraction are presented and discussed next and the paper is closed by concluding remarks.

Author's Accepted Manuscript;
Not Copy-edited by the Journal.

The Green-Naghdi Equations

For an incompressible and inviscid fluid, Green and Naghdi [27] showed that it is possible to derive the governing equations in a systematic way from the exact three-dimensional equations of an incompressible, inviscid fluid (Euler's equations) by use of a single approximation for the (three-dimensional) velocity field. The assumption is equivalent to the Level I assumption in the direct approach, that is the vertical component of the velocity field is a linear function of the vertical coordinate (in a Eulerian system) and that the horizontal components are invariable in the vertical direction. Such a velocity field allows for rotational flow on the horizontal surface, and the vorticity component on the horizontal plane does not need to be zero even though the shear flow on the vertical surfaces are ignored.

We use a Cartesian coordinate system (x_1, x_2, x_3), with the associated orthonormal base vectors e_i, such that the $x_1 - x_3$ plane is the still-water level (SWL) and e_2 is vertically upward. The mass density ρ of the fluid and the gravitational acceleration g, in the $-e_2$ direction, are constant. Subscripts after comma designate partial differentiation with respect to time or the corresponding spatial direction. Ertekin [28] provided a familiar form

 Copyright © by ASME

of the equations given by the mass and momentum conservation as

$$\eta_{,t} + \{(h+\eta-\alpha)u_j\}_{,j} = \alpha_{,t}\,, \quad j = 1,3\,, \tag{1}$$

$$\dot{u}_i + g\eta_{,i} + \frac{\hat{p}_{,i}}{\rho} = -\frac{1}{6}\{[2\eta+\alpha]_{,i}\ddot{\alpha} + [4\eta-\alpha]_{,i}\ddot{\eta} + (h+\eta-\alpha)[\ddot{\alpha}+2\ddot{\eta}]_{,i}\}\,, \quad i = 1,3\,, \tag{2}$$

where $V = u_1e_1 + u_2e_2 + u_3e_3$ is the velocity vector, $\eta(x_1,x_3,t)$ is the free surface elevation measured from the SWL, $\alpha(x_1,x_3,t)$ describes the seafloor surface, and t is the time variable. The scalar function $\hat{p}(x_1,x_3,t)$ is the fluid pressure on the top surface, and $h(x_1,x_3)$ is the water depth (measured from the SWL to the stationary seafloor). The superposed dot denotes the material derivative, and a double superposed dot is defined as the second material time derivative.

Under the GN theory, the vertical velocity, $u_2(x_1,x_2,x_3,t)$, integrated pressure across the water depth, $P(x_1,x_3,t)$, and pressure on the seafloor $\bar{p}(x_1,x_3,t)$ are obtained explicitly by (see e.g. [29, 30])

$$u_2(x_1,x_2,x_3,t) = \dot{\alpha} + \frac{(x_2+h-\alpha)}{(\eta+h-\alpha)}(\dot{\eta}-\dot{\alpha})\,, \tag{3}$$

$$P(x_1,x_3,t) = \left(\frac{\rho}{6}\right)(h+\eta-\alpha)^2(\ddot{\alpha}+2\ddot{\eta}+3g) + \hat{p}\,(h+\eta-\alpha)\,, \tag{4}$$

$$\bar{p}(x_1,x_3,t) = \left(\frac{\rho}{2}\right)(h+\eta-\alpha)(\ddot{\alpha}+\ddot{\eta}+2g) + \hat{p}\,. \tag{5}$$

In this study we confine our attention to cases where (i) the seafloor is stationary, i.e. $\alpha(x_1,x_3,t) = \alpha(x_1,x_3)$, and (ii) pressure is atmospheric on the top surface, i.e. $\hat{p}(x_1,x_3,t) = 0$. The surface elevation, η, is a single-valued function in these equations and hence breaking waves are excluded from this study.

Numerical Solution and Setup

A 3D numerical wave channel is created, where a wavemaker is placed at one end and a wave absorber is located at the opposite end. The numerical wavemaker generates solitary and cnoidal waves of the GN equations, see [28] and [31]. The open-boundary uses Orlanski's condition ([32]) applied to both surface elevation and horizontal velocity to reduce reflections back into the wave tank.

Authors Accepted Manuscript
Not Copy-edited by the Journal.

Copyright © by ASME

The exact nonlinear free surface (kinematic and dynamic) and the seafloor boundary conditions are embedded within the GN equations (1) to (2). On the lateral sides of the wave tank, the channel walls, two types of boundary conditions are enforced, namely the wall condition for no flux normal to the walls, and the radiation condition based on the assumption that the velocity and surface elevation vary smoothly near the lateral boundary to minimize the effect of the lateral walls on the flow field (when the wave refraction and flow in the x_3 direction are remarkable near the wall), see [33] for more details.

The system of equations is solved by use of a central-difference method, second order in space, see [28] for more details. A numerical grid generation is applied to facilitate the use of finite-difference method to solve the equations in the presence of irregular boundaries. This allows the inclusion of irregular boundaries conveniently by mapping the physical domain into a rectangular computational domain. An elliptical mesh generation technique is used, in which a one-to-one mapping is developed between the physical and the computational planes by use of the Laplace equation. A uniform computational grid system with unit interval spacings is used in the solution of all the governing equations, which significantly simplifies the use of the finite-difference method, see [34] for more details.

All problems considered here are symmetric with respect to the $x_1 - x_2$ plane passing through the center line of the domain, and hence only one half of the domain is analyzed by use of the symmetry condition. To avoid numerical instabilities, the bathymetries of the cases considered here are slightly smoothed by taking a weighted average of the depth values of the neighboring points.

Time marching of the solution is achieved iteratively by use of the successive over-relaxation method, see [34] and references therein for more details. Hereafter, all variables are given in dimensionless form by use of ρ, g and h (water depth upwave of the ramp) as a dimensionally independent set. A spatial grid with $\Delta x_1 = \Delta x_3 = 0.4$ is used for domain discretization. A time step of $\Delta t = 0.4$ is used for all calculations, see [33] and [35] for discussion on the grid convergence.

The GN model, discussed in this study, has been verified and validated previously for wave propagation over various forms of uneven bathymetry in two dimensions by [20, 31, 36] for solitary and cnoidal wave propagation over submerged ramps, bumps and mounts. Results of the equations have also been extensively compared with laboratory experiments for wave deformation due to fixed (e.g. [34, 37–39]) or floating bodies (e.g. [40]). In this paper, we will build upon the previous investigations of [33], and confine our attention to the results of the GN model for nonlinear wave diffraction and refraction.

Author's Accepted Manuscript:
Not Copy-edited by the Journal.

Copyright © by ASME

Table 1: Amplitude and width of the ramp curves

Case	FLR	NCR	WCR	NXR	WXR
A_R	0	10	10	-10	-10
B_R	0	12	24	12	24

Results and Discussion

We consider the propagation of nonlinear waves of solitary and cnoidal types over uneven bottom bathymetry. The solitary wave cases provide information about the transformation of very long waves (e.g. tsunami) as they propagate over uneven ocean ramps of various forms into continental shelves. The cnoidal wave cases are considered to investigate the deformation of large oscillatory waves, often generated due to storms and severe atmospheric events, as they propagate over ocean ramps into coastal areas. The shelf consists of a 1:20 flat, linear ramp (FLR hereafter), gradually connecting the constant water depth to shallow region, whose dimensions are shown in Fig. 1. To better investigate the 3D effects and wave refraction, we extend the FLR by adding an additional component across the shelf and consider another four curved-bottom ramps, namely (i) narrow concave ramp (NCR), (ii) wide concave ramp (WCR), (iii) narrow convex ramp (NXR), and (iv) wide convex ramp (WXR), whose dimensions are shown in Fig. 1. The 3D ramp profile, varying both in the x_1 and x_3 directions, is given by $f(x_3) = A_R \cos^2(2\pi x_3/B_R)$ for $x_3 \leq B_R$, where A_R and B_R are the curve amplitude and width of the 3D curves of the ramp, respectively, whose values are given in Table 1 (also shown in Fig. 1). These are similar to those considered by [35], who used Boussinesq-class equations to study the wave refraction and diffraction. The 3D ramps, while allow us to perform a systematic analysis of the effect of uneven bathymetry on wave transformation, resemble various real-life cases of wave propagation from deep to shallow water.

In all cases, computations are performed in 3D, and the domain length is 120, extending from $x_1 = -30$ to $x_1 = 90$, and its width is 32, from $x_3 = -16$ to $x_3 = 16$. $x_3 = 0$, the center line of the bathymetry, is the line of symmetry in all cases. The ramp starts from $x_1 = 6$, and the water depth on the shelf (downwave of the ramp) is always $h_1 = 0.5$.

Solitary Waves

The solitary wave amplitude is kept constant in all cases considered in this study at $A = 0.12$. The 3D surface elevation of the waves propagating over the five ramps is shown in Fig. 2. The color bar remains unchanged in all cases for better comparisons. The wave profile undergoes significant deformation as it propagates over the

Author's Accepted Manuscript, Not Copy-edited by the Journal.

Copyright © by ASME

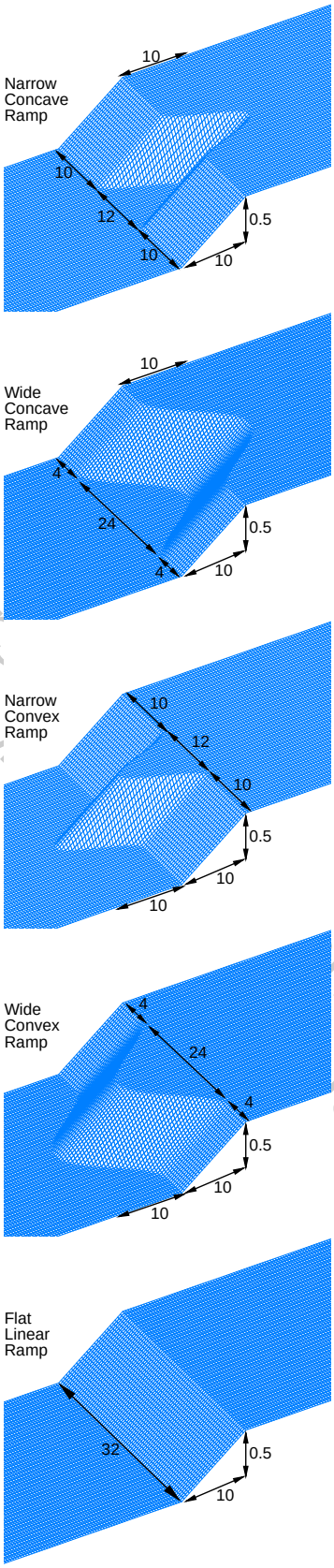

Author-
Not Copy
nuscript,
Journal.

Fig. 1: Schematic of the five deep-to-shallow ramps considered in this study, and their dimensions. Not to scale.

Copyright © by ASME

shelves.

The nonlinearity parameter, σ, is physically manifested as the tendency of the wave front to steepen during the propagation, while the dispersion parameter, ε, gauges the tendency of a single wave to disperse into a train of oscillatory waves. The relative magnitude of these two parameters, the Ursell number $Ur = \sigma/\varepsilon^2$, is often used to determine which phenomenon (nonlinearity or dispersion) dominates during wave transformation, see [41]. The solitary wave is stable when the two parameters are in balance, i.e. $Ur = O(1)$. The change in the bathymetry breaks this balance locally, and hence the wave undergoes deformation to achieve a new stable form.

As the wave approaches the ramp, part of the mass and energy is reflected back, and the wave deformation begins. The water depth reduces as the wave propagates over the ramp and onto the shelf, resulting in increasing nonlinearity. Hence, in all cases, the amplitude of the main soliton is larger immediately downwave of the shelf. As the wave propagates away from the shelf, dispersion comes into play and results in the formation of second and third solitons, which separate from the main wave as it propagates over the constant water depth above the shelf. The form of the 3D shelf, of course, plays an important role on the exact form and amplitude of the solitons.

Comparing results of the FLR case to the other four clearly shows the 3D effects, causing asymmetry of the wave profile from the center line ($x_3 = 0$) to the wall of the domain ($x_3 = 16$), best seen in snapshots taken at times $t = 30$ and 60 in Fig. 2 (a) - (d). In the concave ramp cases, NCR and WCR, the amplitude of the main soliton becomes larger along the wall, while for the convex cases, NXR and WXR, the main soliton's peak is amplified along the centerline of the domain. This is in line with the classic wave refraction theories (see e.g. [42]), where the lines parallel to the wave crest, obliquely approaching a ramp, turn direction such that the angle between the crest line and the depth contours become smaller, i.e., Snell's law. Similarly, in the 3D ramps, the ray lines (lines perpendicular to the 3D wave crest pointing to the wave propagation direction) turn towards shallower water as the wave passes over the curved ramp.

The cases with wider curved ramps, WCR and WXR, cause larger differences of the wave amplitude across the channels when compared to the cases with narrower ramps, NCR and NXR. Downwave from the shelf and over the constant water depth, the balance between nonlinearity and dispersion is achieved once again and the wave profile becomes nearly identical across the channel, best seen in snapshots taken at time $t = 60$ in Fig. 2 (a) -(d).

To better assess the effect of the uneven seafloor on the wave field, we look at the snapshots of the horizontal and vertical velocities in Figs. 3 and 4, respectively, at the free surface taken at the same four different times. Shown in Fig. 3, in all cases, the horizontal velocity is at its maximum value under the wave crest, with higher

Author's Accepted Manuscript;
Not Copy-edited by the Journal.

Copyright © by ASME

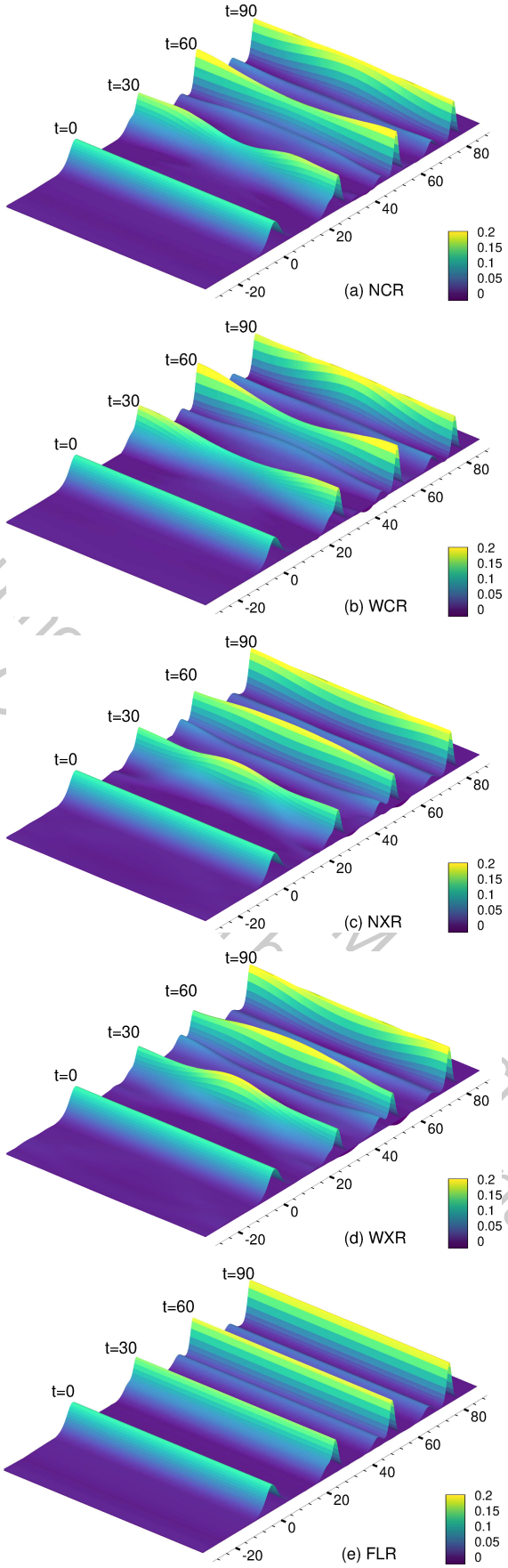

Fig. 2: Snapshots of the surface elevation of a solitary wave propagating over (a) NCR, (b) WCR, (c) NXR, (d) WXR, and (e) FLR. The ramp starts from $x_1 = 6$. The snapshots are taken at four different times, but plotted on the same figure.

Copyright © by ASME

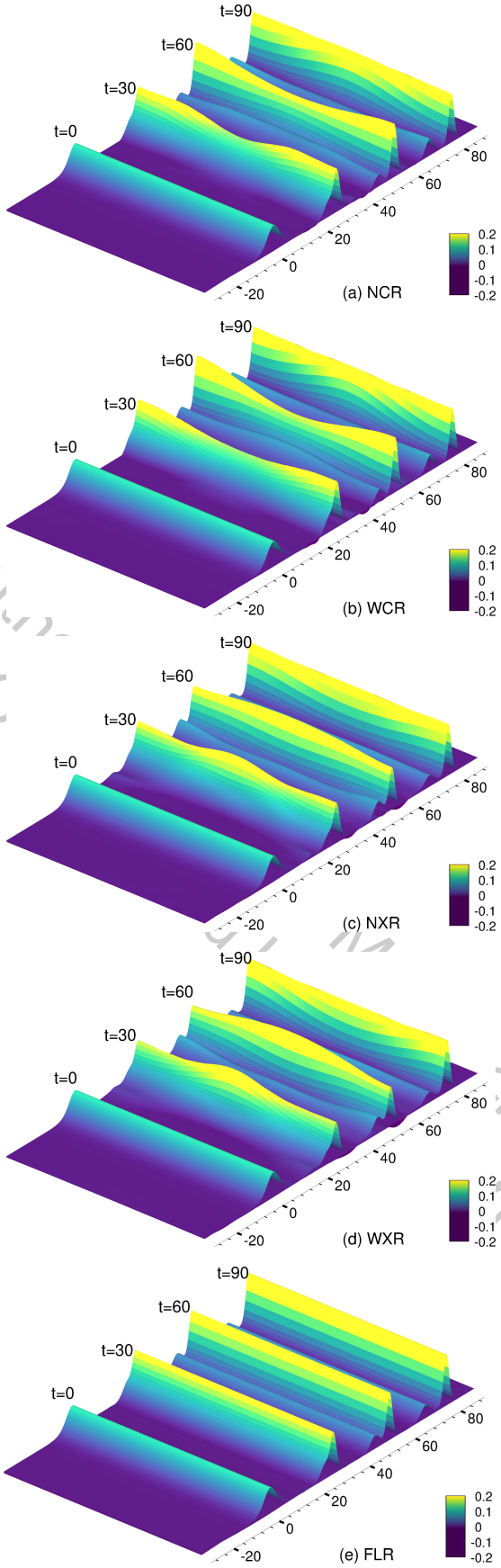

Fig. 3: Snapshots of the horizontal velocity of a solitary wave propagating over (a) NCR, (b) WCR, (c) NXR, (d) WXR, and (e) FLR. The snapshots are taken at four different times, but plotted on the same figure. The color bars are kept the same in all figures to allow for better comparisons between cases.

Copyright © by ASME

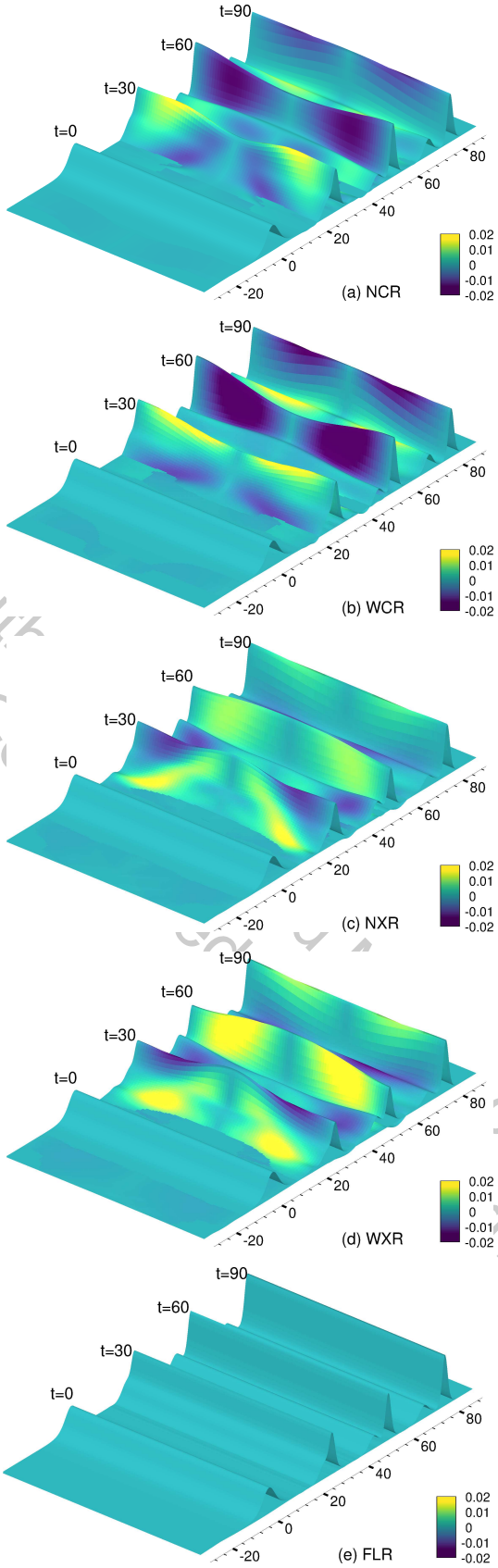

Fig. 4: Snapshots of the vertical velocity of a solitary wave propagating over (a) NCR, (b) WCR, (c) NXR, (d) WXR, and (e) FLR. The snapshots are taken at four different times, but plotted on the same figure. The color bars are kept the same in all figures to allow for better comparisons between cases.

Copyright © by ASME

magnitudes where the surface elevation is larger. For the most part, the distribution of the horizontal velocity has remained invariant by the submerged ramps. When compared to the flat linear ramp (FLR), the distribution of the vertical velocity is asymmetric from the center line of the channel to the channel walls, see Fig. 4. As the wave deforms, in the concave cases, NCR and WCR, areas of negative vertical velocity is observed at the back of the wave (best seen at time $t = 60$ in Fig. 4 (a) and (b)), which have larger magnitudes in the wider ramp case, WCR. The opposite is observed in these regions for the convex cases, i.e. larger positive vertical velocities, which are more remarkable in the wider ramp case, WXR. The horizontal velocity is always larger in areas with larger surface elevation.

To better investigate the change in the wave profile across the width of the channels (due to the curved ramps), in Figs. 5 to 9, we look at snapshots of surface elevation along the center line and the wall of the channel. We keep the height of the vertical axis the same in all these figures for better comparison. In all cases, as mentioned earlier, the front side of the wave steepens and the wave amplitude grows as the wave approaches the ramp. Downwave over the shelf, soliton fission is observed, where two or three solitons are formed and as the wave propagates, separate from the leading soliton due to differences in their propagation velocity (note that the soliton speed predicted by the present theory is $U = \sqrt{1+A}$, always critical or supercritical, see [20] and references cited therein).

When compared to the FLR case, in all curved cases, there is a remarkable difference between the wave profile at the center of the domain versus that at the channel wall, best seen at times $t = 40$ and 60 in Figs. 5-8, which, is due to the wave refraction by different curved bathymetries. In the concave cases, NCR and WCR, , where middle of the shelf is deeper than the edges, the wave amplitude is larger near the wall, and the opposite is observed for the convex cases, NXR and WXR. At the later stages of soliton propagation over the shelf, $t = 80$ in Figs. 5-8, the amplitude of the main soliton is nearly identical at the center and wall cut of the channel. The amplitude of the second and third solitons, however, are different at the center and wall cut of the channel even at $t = 80$; in the concave cases, the amplitude of the second soliton is larger at the center line, while the opposite is observed in the convex cases (where the sides of the ramp are deeper than the middle part). Similarly, in the concave cases, at time $t = 80$, the second soliton is separated from the main soliton at the center line of the domain while it is still part of the main soliton at the channel wall. In the convex cases, the opposite is observed due to the shape of the ramp, i.e., the second soliton at the wall is separated, but not at the center line. Shown in Figs. 5-9, results of the GN equations are in very good agreement with those obtained by [35] who used the Boussinesq equations.

A comparison of the amplitudes of the first (A_1) and second (A_2) solitons, generated due to the propagation of a

Author's Accepted Manuscript;
Not Copy-edited by the Journal.

Copyright © by ASME

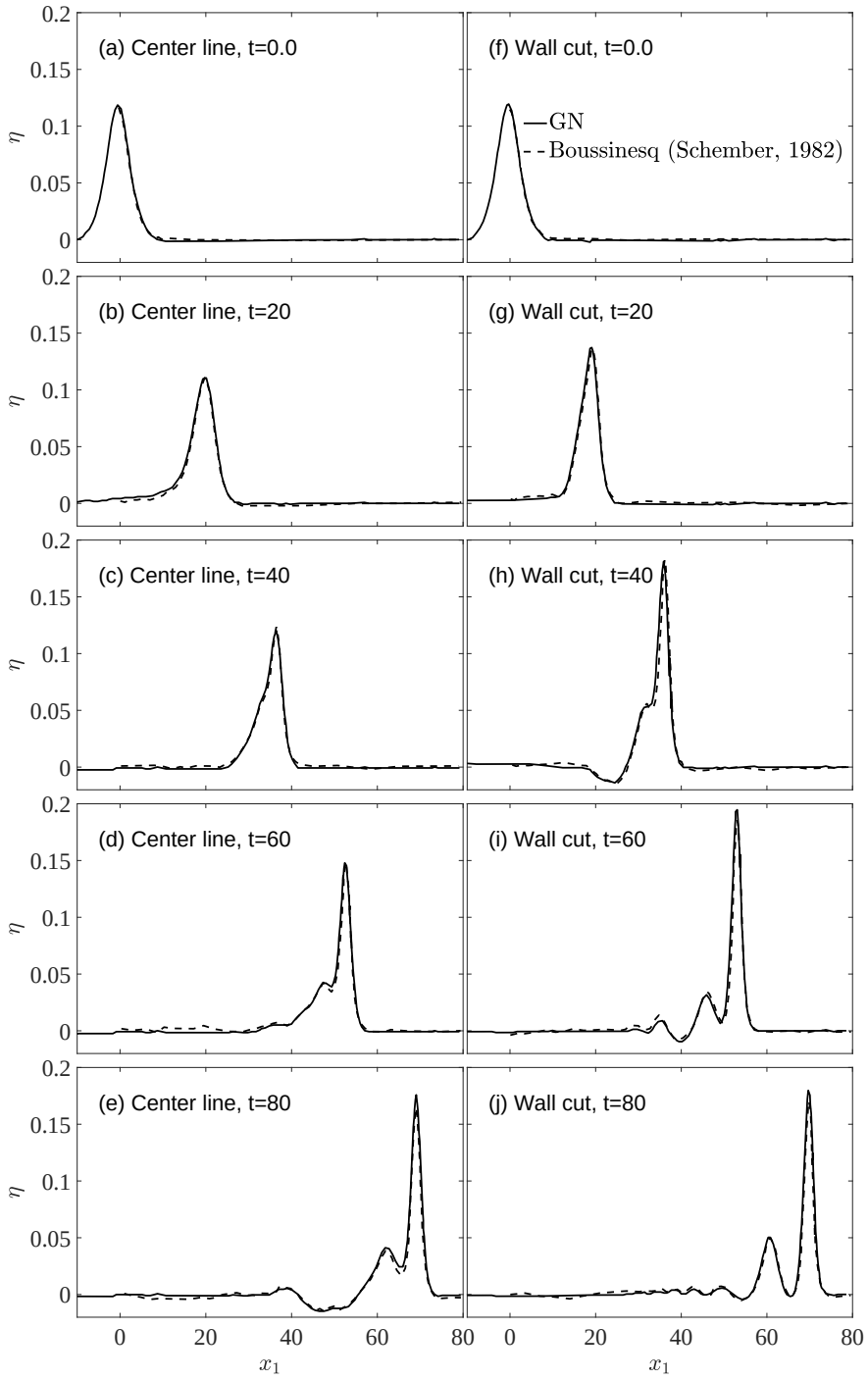

Fig. 5: Snapshots of surface elevation of solitary wave propagating over the narrow concave ramp (NCR) at the center line (a-e) and wall cut (f-j), calculated by the GN model and compared with the Boussinesq-class results of [35].

Copyright © by ASME

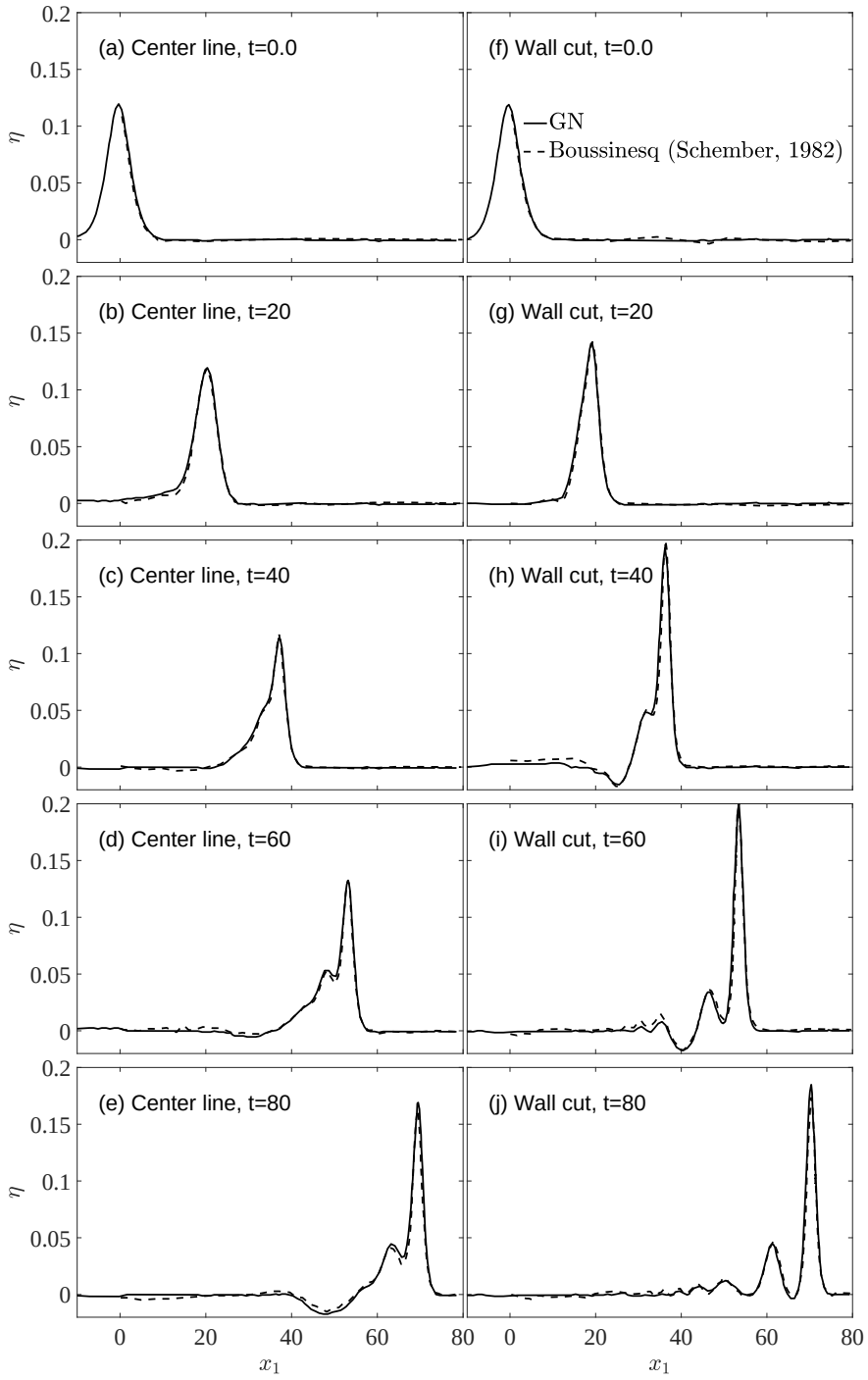

Fig. 6: Snapshots of surface elevation of solitary wave propagating over the wide concave ramp (WCR) at the center line (a-e) and wall cut (f-j), calculated by the GN model and compared with the Boussinesq-class results of [35].

Copyright © by ASME

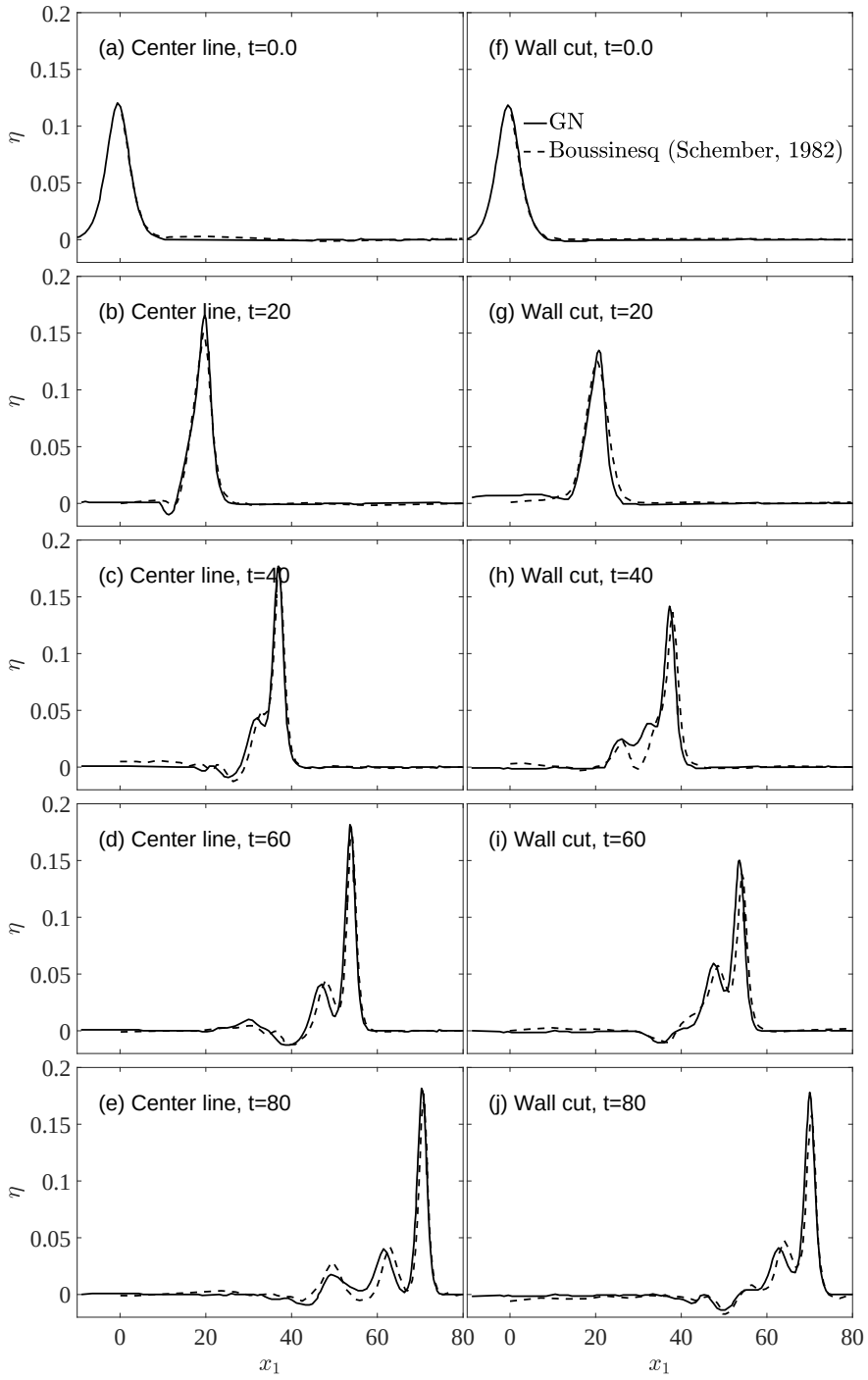

Fig. 7: Snapshots of surface elevation of solitary wave propagating over the narrow convex ramp (NXR) at the center line (a-e) and wall cut (f-j), calculated by the GN model and compared with the Boussinesq-class results of [35].

Copyright © by ASME

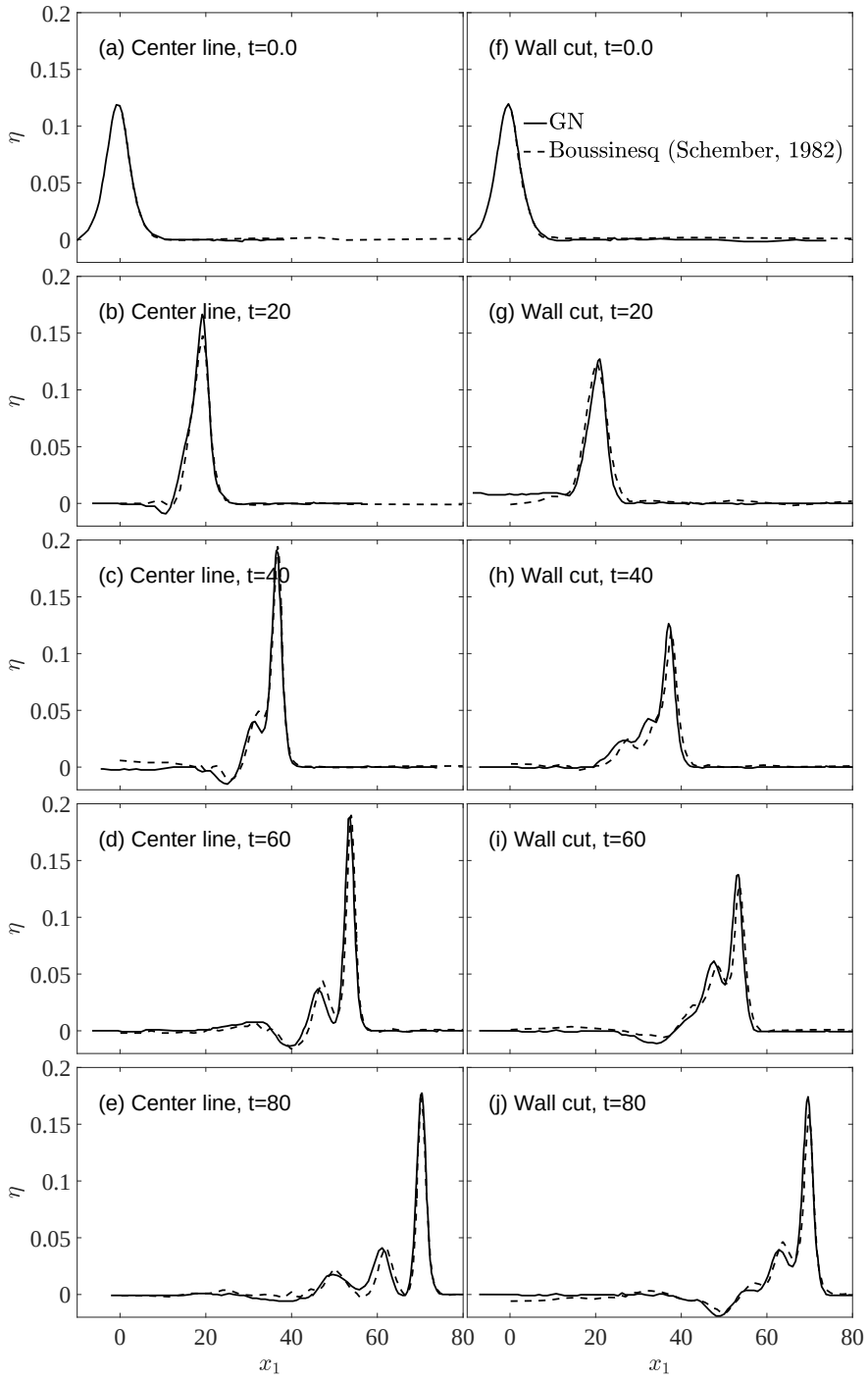

Fig. 8: Snapshots of surface elevation of solitary wave propagating over the wide convex ramp (WXR) at the center line (a-e) and wall cut (f-j), calculated by the GN model and compared with the Boussinesq-class results of [35].

Copyright © by ASME

Table 2: Comparison of the amplitudes of the first (A_1) and second (A_2) solitons due to propagation of a solitary wave over a flat linear ramp, obtained by various approaches. A is the initial amplitude of the solitary wave.

Results	A_1/A	A_2/A
Madsen and Mei 1969 (Experiments)	1.2	0.4
Madsen and Mei 1969 (Boussinesq)	1.66	0.75
Johnson 1972 (KdV)	1.71	0.66
Johnson 1973 (Analytical)	1.73	0.65
Schember 1982 (Boussinesq)	1.69	0.59
GN	1.60	0.45

Authors Accepted Manuscript, Not copy edited by the Journal.

solitary wave over FLR (shown in Fig. 9) of the GN equations and those obtained through laboratory experiments and calculations of [5, 35, 43] is given in Table 2. The amplitudes are recorded at approximately $x_1 = 33$ from the leading edge of the shelf. Results are also in good agreement overall with the laboratory measurements of Madsen and Mei [5] and calculations of Johnson [43, 44] (using numerical solution of the KdV equations, as well as formal asymptotic expansions to obtain analytical expressions for the number of solitons and their amplitudes as a function of the ramp height and the initial wave amplitude). The peak of the soliton calculated by the GN equations are slightly smaller than those reported by [43, 44], mainly because wave reflection (as large as about 15% in this case, see [20]) is neglected in the KdV models. Note the difference of all theoretical results when compared to the laboratory experiments of Madsen and Mei [5], although the GN equations are the closest among all theoretical solutions. [5] attributed the differences between the numerical and experimental results possibly to the use of an approximate wave generation technique in the laboratory experiments. In this regard, it may be a good idea to repeat these experiments in the future.

Cnoidal Wave

In this section, results of the GN model for cnoidal wave propagation over the five bottom ramps are presented. The dimensionless wave height and wavelength are $H = 0.12$ and $\lambda = 20$, respectively. All other variables and numerical setup are identical to those discussed in the previous sections. Snapshots of the 3D surface elevation and plane contour views of cnoidal waves propagating over these ramps obtained by the GN model are shown in Fig. 10. The cnoidal waves deform significantly as they propagate over the ramp into the shelf, and this varies in different cases. Qualitatively, similar behaviour in wave diffraction and refraction is observed as those of a solitary wave, with the difference that the incoming waves undergo further deformation due to the interaction

Copyright © by ASME

with the reflected waves (as several waves are present in the domain at a given time), and with waves of smaller amplitudes.

Seen in the plane contour view of Fig. 10 (a) and (b), the concave ramps have caused slower wave propagation in the center of the domain when compared to the edges of the domain. In the case of convex ramps, however, the wave propagates faster in the centre of the domain, observed in Fig. 10 (c) and (d). Downwave from the ramp, and on the shelf with constant water depth, the wave crest gradually recovers into a uniform wave across the domain width.

To further investigate the cnoidal wave diffraction and refraction by the submerged ramps, in Fig. 11, snapshots of surface elevation at the center of the domain is compared with that at the wall cut, for all five cases considered here. Deviation between surface elevations at the center and the wall cuts is observed from approximately $x_1 = 0$, just upwave of the ramp. The concave ramps have resulted in smaller wave amplitudes at the centre of the domain and larger amplitudes near the walls, seen in Fig. 11 (a) and (b). The convex ramps have opposite effect on the change of the wave amplitude across the domain width, i.e., the wave amplitude in the center of the domain is larger than that near the walls, shown in Fig. 11 (c) and (d). The change in wave amplitude is invariant with the domain width for the linear flat ramp (Fig. 11 (e)), and this is expected. Higher harmonics are generated due to the propagation of the waves over the ramps, the amplitude of which varies across the width of the domain and dependent on the shape of the ramps (concave vs convex). Downwave on the shelf, the main wave peak separates itself from the second harmonic.

Author's Accepted Manuscript;
Not Copy-edited by the Journal.

Concluding Remarks

A 3D model for nonlinear wave propagation in shallow water and over uneven bathymetry is developed based on the Level I GN equations. A 3D numerical wave tank is created and a flat, linear ramp is considered in this study. To further investigate the 3D effects on the wave refraction, four extensions are added systematically to the flat shelf, creating concave and convex ramps of different widths. The model is used to study solitary and cnoidal wave diffraction and refraction due to various forms of 3D bathymetry that are observed in real-life.

Through the results obtained from the GN model, it is observed that the waves undergo significant deformation as they propagate over the ramps. Common across all cases, the wave amplitude initially increases due to the stronger nonlinearity. The growth of the wave amplitude across the channel width varies depending on the shape of the ramp, such that for concave cases, the wave amplitude is larger at the channel walls, while the wave in the center line is larger for the convex cases. Downwave of the ramp, soliton fission is observed, where second (and

Copyright © by ASME

sometimes third) solitons are formed. Again the shape of the bathymetry has a significant effect on the magnitude of the second (and third) solitons.

It is concluded that the GN equations, capturing nonlinearity, dispersion and wave reflection, which also satisfy the boundary conditions exactly, are a remarkable alternative to perturbation-based methods, and a very efficient alternative to computational fluid dynamics models to study wave transformation in coastal areas.

Authors Accepted Manuscript;
Not Copy-edited by the Journal.

Copyright © by ASME

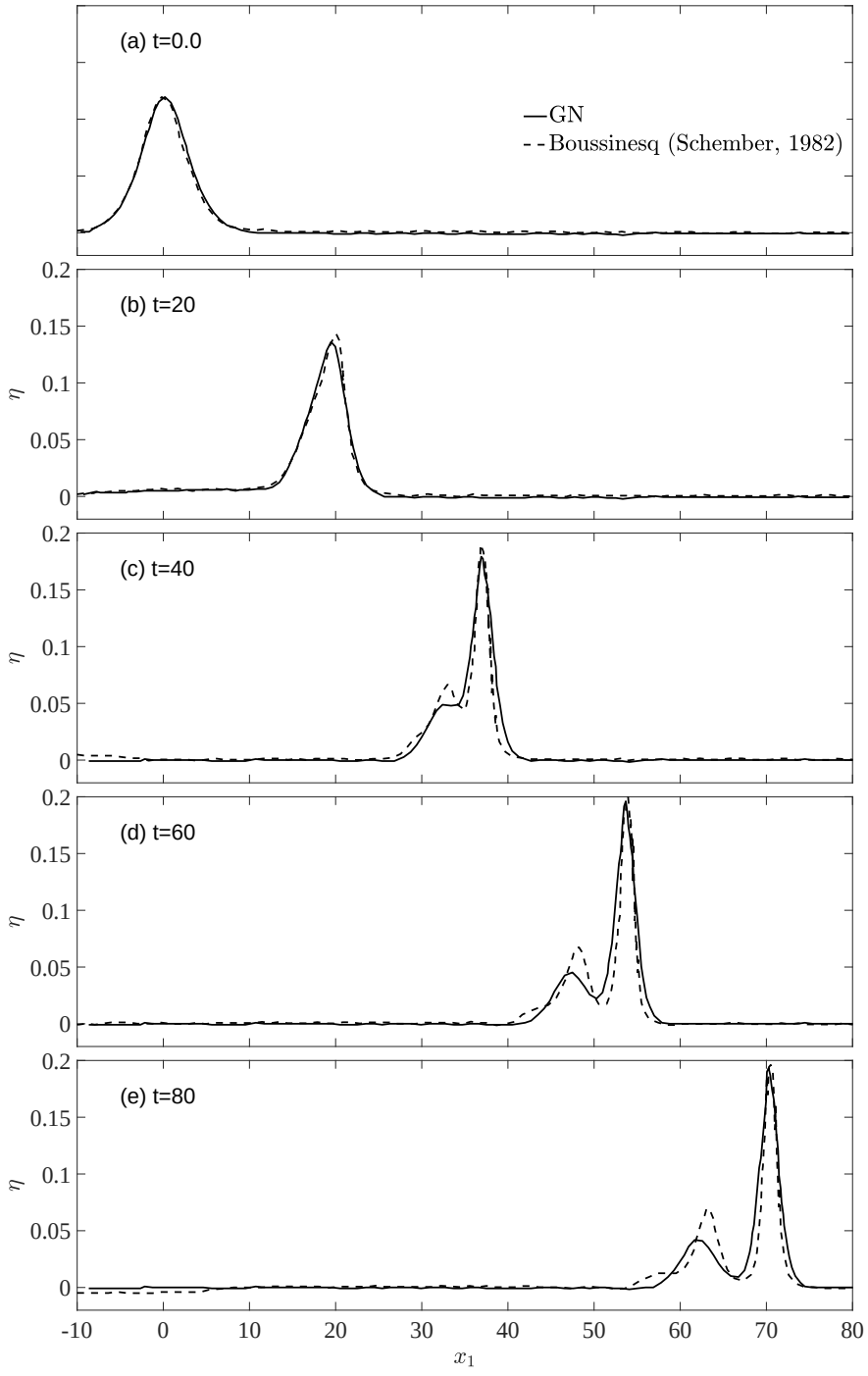

Fig. 9: Snapshots of surface elevation of solitary wave propagating over the flat linear ramp (FLR), calculated by the GN model and compared with the Boussinesq-class results of [35].

Copyright © by ASME

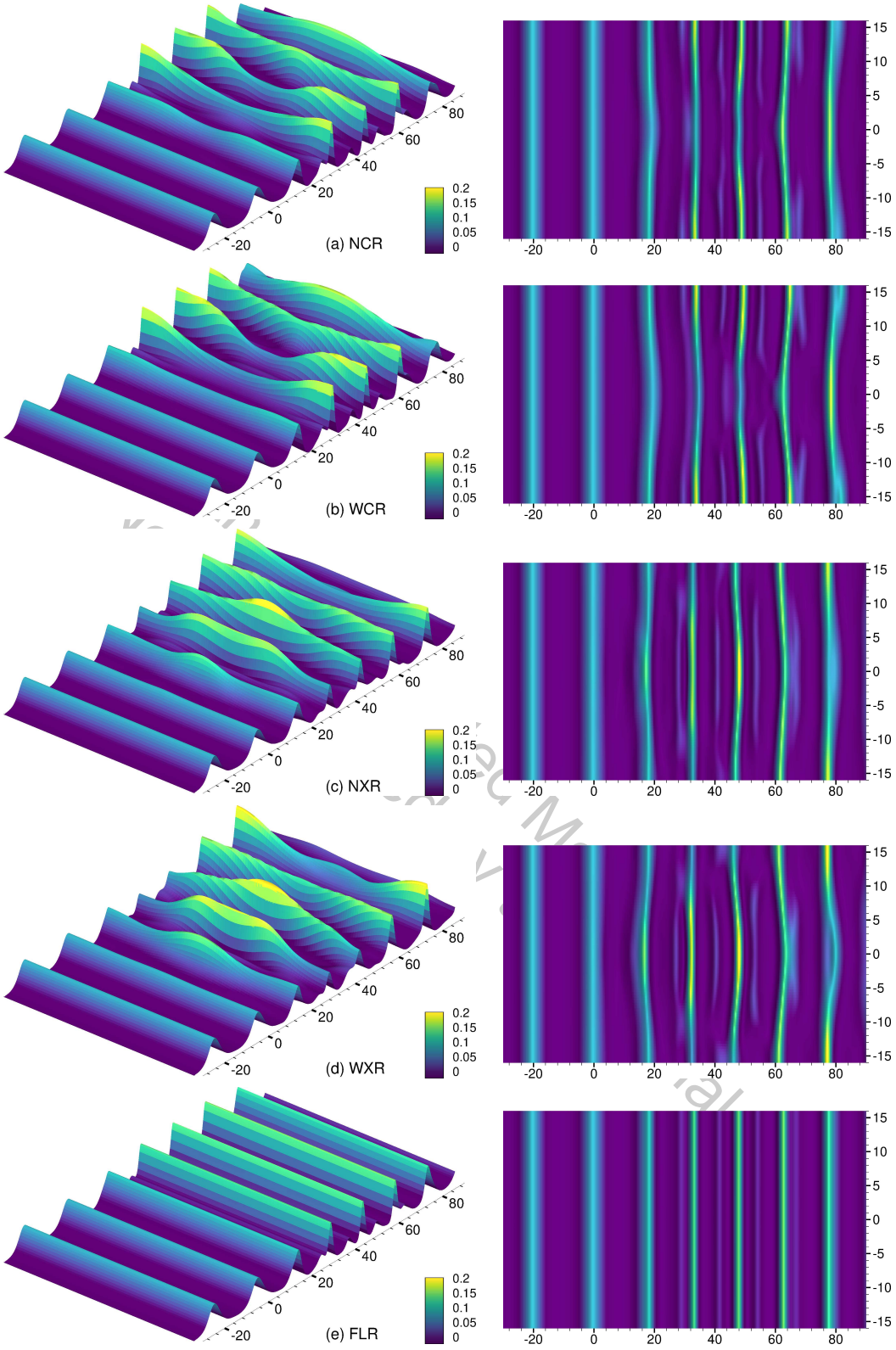

Fig. 10: 3D (left column) and contour plain view (right column) snapshots of the surface elevation of cnoidal waves propagating over (a) NCR, (b) WCR, (c) NXR, (d) WXR, and (e) FLR, taken at time t=200. The ramp starts from $x_1 = 6$.

Copyright © by ASME

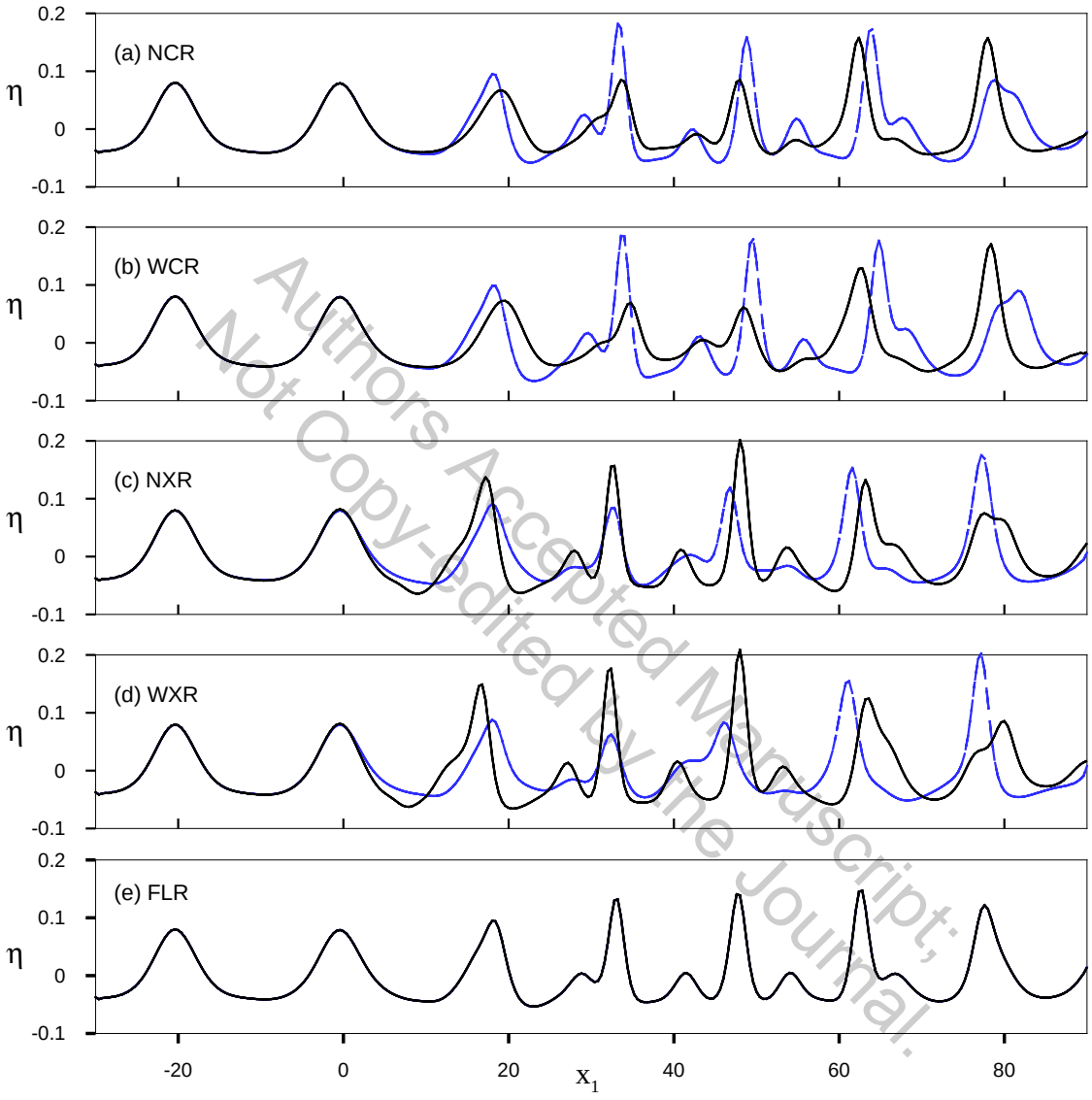

Authors Accepted Manuscript; Not Copy-edited by the Journal.

Fig. 11: Snapshots of surface elevation of cnoidal waves propagating over the (a) NCR, (b) WCR, (c) NXR, (d) WXR, and (e) FLR, at the centre line (black solid line) and wall cut (blue dash line) of the domain, taken at time t=200.

Copyright © by ASME

References

[1] Boussinesq, J., 1871. "Théorie de l'intumescence liquide appelée onde solitaire ou de translation". *Comptes Rendus de l'Académie des Sciences,* ***72***, pp. 755–759.

[2] Rayleigh, L., 1876. "On waves". *Philosophical Magazine,* ***1***(4), pp. 257–279.

[3] Korteweg, D., and de Vries, G., 1895. "On the change of form of long waves advancing in a rectangular canal, and on a new type of long stationary waves". *Philosophical Magazine,* ***39***(5), pp. 422–443.

[4] Laitone, E., 1960. "The second approximation to cnoidal and solitary waves". *Journal of Fluid Mechanics,* ***9***(3), pp. 430–444.

[5] Madsen, O. S., and Mei, C. C., 1969. "The transformation of a solitary wave over an uneven bottom". *Journal of Fluid Mechanics,* ***39***(4), pp. 781–791.

[6] Grimshaw, R., 1971. "The solitary wave in water of variable depth. part 2". *Journal of Fluid Mechanics,* ***46***(3), pp. 611–622.

[7] Fenton, J., 1972. "A ninth-order solution for the solitary wave". *Journal of Fluid Mechanics,* ***53***(2), pp. 257–271.

[8] Wu, T., 1981. "Long waves in ocean and coastal waters". *Journal of the Engineering Mechanics Division,* ***107***(3), May/June, pp. 501–522.

[9] Liu, P. L.-F., and Losada, I. J., 2002. "Wave propagation modeling in coastal engineering". *Journal of Hydraulic Research,* ***40***(3), pp. 229–240.

[10] Choi, D. Y., and Wu, C. H., 2006. "A new efficient 3D non-hydrostatic free-surface flow model for simulating water wave motions". *Ocean Engineering,* ***33***(5-6), pp. 587–609.

[11] Zhu, S.-P., and Harun, F. N., 2009. "An analytical solution for long wave refraction over a circular hump". *Journal of Applied Mathematics and Computing,* ***30***(1), pp. 315–333.

[12] Young, C.-C., Wu, C. H., Liu, W.-C., and Kuo, J.-T., 2009. "A higher-order non-hydrostatic σ model for simulating non-linear refraction–diffraction of water waves". *Coastal Engineering,* ***56***(9), pp. 919–930.

[13] Engsig-Karup, A. P., Bingham, H. B., and Lindberg, O., 2009. "An efficient flexible-order model for 3D nonlinear water waves". *Journal of Computational Physics,* ***228***(6), pp. 2100–2118.

[14] Yamazaki, Y., Kowalik, Z., and Cheung, K. F., 2009. "Depth-integrated, non-hydrostatic model for wave breaking and run-up". *International Journal for Numerical Methods in Fluids,* ***61***(5), pp. 473–497.

[15] Roeber, V., Cheung, K. F., and Kobayashi, M. H., 2010. "Shock-capturing Boussinesq-type model for nearshore wave processes". *Coastal Engineering,* ***57***(4), pp. 407–423.

Authors Accepted Manuscript; Not Copy-edited by the Journal.

Copyright © by ASME

[16] Ma, G., Shi, F., and Kirby, J. T., 2012. "Shock-capturing non-hydrostatic model for fully dispersive surface wave processes". *Ocean Modelling,* ***43***, pp. 22–35.

[17] Green, A. E., and Naghdi, P. M., 1974. "On the theory of water waves". *Proceedings of the Royal Society of London. Series A, Mathematical and Physical Sciences,* ***338***(1612), pp. 43–55.

[18] Shields, J. J., and Webster, W. C., 1988. "On direct methods in water-wave theory". *J. Fluid Mechanics,* ***197***, pp. 171–199.

[19] Bonneton, P., Barthélemy, E., Chazel, F., Cienfuegos, R., Lannes, D., Marche, F., and Tissier, M., 2011. "Recent advances in Serre–Green–Naghdi modelling for wave transformation, breaking and runup processes". *European Journal of Mechanics-B/Fluids,* ***30***(6), pp. 589–597.

[20] Ertekin, R. C., Hayatdavoodi, M., and Kim, J. W., 2014. "On some solitary and cnoidal wave diffraction solutions of the Green-Naghdi equations". *Applied Ocean Research,* ***47***, pp. 125–137.

[21] Zhao, B. B., Duan, W. Y., Ertekin, R. C., and Hayatdavoodi, M., 2015. "High-level Green–Naghdi wave models for nonlinear wave transformation in three dimensions". *Journal of Ocean Engineering and Marine Energy,* ***1***(2), pp. 121–132.

[22] Zhang, Y., Kennedy, A. B., Tomiczek, T., Donahue, A., and Westerink, J. J., 2016. "Validation of boussinesq–green–naghdi modeling for surf zone hydrodynamics". *Ocean Engineering,* ***111***, pp. 299–309.

[23] Zhao, B. B., Ertekin, R. C., Duan, W. Y., and Hayatdavoodi, M. H., 2014. "On the steady solitary-wave solution of the Green-Naghdi equations of different levels". *Wave Motion,* ***51***(8), pp. 1382–1395.

[24] Webster, W. C., and Zhao, B. B., 2018. "The development of a high-accuracy, broadband, Green–Naghdi model for steep, deep-water ocean waves". *Journal of Ocean Engineering and Marine Energy,* ***4***(4), pp. 273–291.

[25] Zhao, B. B., Zhang, T. Y., Wang, Z., Duan, W. Y., Ertekin, R. C., and Hayatdavoodi, M., 2019. "Application of three-dimensional IGN-2 equations to wave diffraction problems". *Journal of Ocean Engineering and Marine Energy,* ***5***(4), pp. 351–363.

[26] Zhao, B. B., Wang, Z., Duan, W., Ertekin, R. C., Hayatdavoodi, M., and Zhang, T., 2020. "Experimental and numerical studies on internal solitary waves with a free surface". *Journal of Fluid Mechanics,* ***899***, p. A17.

[27] Green, A. E., and Naghdi, P. M., 1976. "A derivation of equations for wave propagation in water of variable depth". *Journal of Fluid Mechanics,* ***78***, 10, pp. 237–246.

[28] Ertekin, R. C., 1984. "Soliton generation by moving disturbances in shallow water: Theory, computation and experiment". PhD thesis, University of California at Berkeley, May, v+352 pp.

Author's Accepted Manuscript.
Not Copy-edited by the Journal.

Copyright © by ASME

[29] Ertekin, R. C., Webster, W. C., and Wehausen, J. V., 1986. "Waves caused by a moving disturbance in a shallow channel of finite width". *Journal of Fluid Mechanics,* ***169***, 7, pp. 275–292.

[30] Hayatdavoodi, M., and Ertekin, R. C., 2015. "Wave forces on a submerged horizontal plate. Part I: Theory and modelling". *Journal of Fluids and Structures,* ***54***(April), pp. 566–579.

[31] Ertekin, R. C., and Becker, J. M., 1998. "Nonlinear diffraction of waves by a submerged shelf in shallow water". *Journal of Offshore Mechanics and Arctic Engineering,* ***120***, November, pp. 212–220.

[32] Orlanski, I., 1976. "A simple boundary condition for unbounded hyperbolic flows". *Journal of computational physics,* ***21***(3), pp. 251–269.

[33] Ertekin, R. C., and Sundararaghavan, H., 2003. "Refraction and diffraction of nonlinear waves in coastal waters by the level I Green-Naghdi equations". In Proc. 22nd Int. Conf. on Offshore Mechanics and Arctic Engineering, OMAE '03, ASME, Cancun, Mexico, p. 10.

[34] Hayatdavoodi, M., Neill, D. R., and Ertekin, R. C., 2018. "Diffraction of cnoidal waves by vertical cylinders in shallow water". *Theoretical and Computational Fluid Dynamics,* ***32***(5), pp. 561–591.

[35] Schember, H. R., 1982. "A new model for three-dimensional nonlinear dispersive long waves". PhD thesis, California Institute of Technology, Pasadena, CA.

[36] Ertekin, R. C., and Wehausen, J. V., 1986. "Some soliton calculations". In *Proc. 16th Symp. on Naval Hydrodynamics, Berkeley*. Ed. by W.C. Webster, National Academy Press, Washington, D.C., 1987, pp. 167–184.

[37] Hayatdavoodi, M., and Ertekin, R. C., 2015. "Wave forces on a submerged horizontal plate. Part II: Solitary and cnoidal waves". *Journal of Fluids and Structures,* ***54***(April), pp. 580–596.

[38] Hayatdavoodi, M., and Ertekin, R. C., 2015. "Nonlinear wave loads on a submerged deck by the Green-Naghdi equations". *Journal of Offshore Mechanics and Arctic Engineering,* ***137***(1), pp. 011102 (1–9).

[39] Hayatdavoodi, M., Treichel, K., and Ertekin, R. C., 2019. "Parametric study of nonlinear wave loads on submerged decks in shallow water". *Journal of Fluids and Structures,* ***86***, pp. 266–289.

[40] Kostikov, V. K., Hayatdavoodi, M., and Ertekin, R. C., 2021. "Drift of elastic floating ice sheets by waves and current, part I: single sheet". *Proceedings of Royal Society A,* ***477***, p. 20210449.

[41] Ursell, F., 1953. "The long-wave paradox in the theory of gravity waves". *Mathematical Proceedings of the Cambridge Philosophical Society,* ***49***(4), pp. 685–694.

[42] Dhanak, M. R., and Xiros, N. I., 2016. *Springer Handbook of Ocean Engineering*. Springer.

[43] Johnson, R. S., 1972. "Some numerical solutions of a variable-coefficient Korteweg-de Vries equation (with

Author's Accepted Manuscript.
Not Copy-edited by the Journal.

 Copyright © by ASME

applications to solitary wave development on a shelf)". *Journal of Fluid Mechanics,* ***54***, 6, pp. 81–91.

[44] Johnson, R. S., 1973. "On the development of a solitary wave moving over an uneven bottom". *Mathematical Proceedings of the Cambridge Philosophical Society,* ***73***(1), pp. 183–203.

Authors Accepted Manuscript;
Not Copy-edited by the Journal.

Copyright © by ASME